# Analyst

Accepted Manuscript






ROYAL SOCIETY OF CHEMISTRY

www.rsc.org/analyst

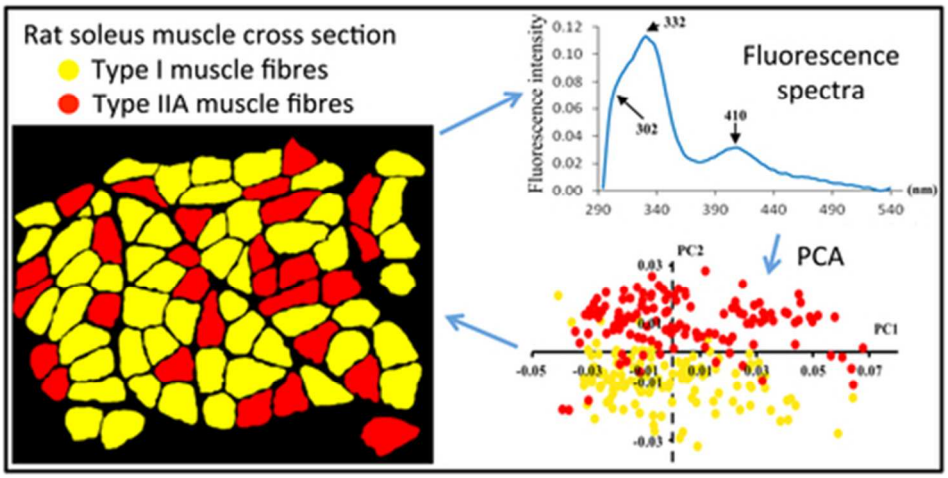


DUV autofluorescence microspectroscopy allows label free fibre typing in muscles.

39x19mm (300 x 300 DPI)

Cite this: DOI: 10.1039/c0xx00000x

www.rsc.org/xxxxxx

ARTICLE TYPE

# Deep UV excited muscle cell autofluorescence varies with the fibre type

**Caroline Chagnot[a, b], Annie Vénien[a], Frédéric Peyrin[a], Frédéric Jamme[c, d], Matthieu Réfrégiers[c], Mickaël Desvaux[b] and Thierry Astruc*[a]**

***Received (in XXX, XXX) Xth XXXXXXXXX 20XX, Accepted Xth XXXXXXXXX 20XX***
**DOI: 10.1039/b000000x**

The rat skeletal muscle consists of four pure types of muscle cells called type I, type IIA, type IIX and type IIB, and their hybrids in different proportions. They differ in their contraction speeds and metabolic pathways. Intracellular composition is adapted to the fibre work and therefore to fibre types. Given that small differences in composition are likely to alter the optical properties of the cells, we studied the impact of cell type on the fluorescent response following excitation in deep UV. Rat soleus and extensor digitorum longus (EDL) muscle fibres, previously identified on their cell types by immunohistofluorescence, were analyzed by synchrotron fluorescence microspectroscopy on stain-free serial muscle cross sections. Muscle fibres excited at 275 nm showed differences in fluorescence emission intensity among fibre types at 302, 325, 346 and 410 nm. The 410/325 ratio decreased significantly with contractile and metabolic features in EDL muscle, ranked I>IIA>IIX>IIB fibres ($p<0.01$). Compared to type I fibres, the 346/302 ratio of IIA fibres decreased significantly in both EDL and soleus muscles ($p < 0.01$). This study highlights the usefulness of autofluorescence spectral signals to characterize histological cross section of muscle fibres with no staining chemicals.

## Introduction

Skeletal muscle contains about 75% water, 19% protein, 0.5–8% lipid and 1% glycogen, and is composed of several tissues such as myofibres, connective tissue, intramuscular adipocytes, vascular and nervous tissues. Myofibres, which represent 75–90% of the muscle volume, show a heterogeneous population differing in structural, contractile, metabolic and physiological properties [1, 2]. Myofibres are generally divided into four types, called type I, type IIA, type IIX and type IIB [2-4]. Type I and IIA have an oxidative metabolism, with $H_2O$ and $CO_2$ as final products, while type IIX and IIB use a glycolytic metabolism, where pyruvate is anaerobically fermented into lactic acid. Myofibres are also characterized by their speed of contraction, ranked I < IIA < IIX < IIB [5, 6].

Metabolic enzyme and structural protein compositions are adapted to physiological function, and so to the fibre type. Type I and IIA oxidative metabolism fibres have a high content of myoglobin and mitochondria, and so a higher content of oxidative phosphorylation enzymes [3, 7] and cofactors of the respiratory chain, such as NADH [8, 9]. Conversely, IIX and IIB fibres have low levels of myoglobin and mitochondria, but higher levels of enzyme of the glycolysis chain [3, 7]. Many differences in gene expression can be observed when comparing different fibre types [4, 7, 10], suggesting numerous differences in protein composition depending on the fibre type. The underlying molecular basis of this muscle fibre typology is the polymorphism of the myosin heavy chains (MyHC). Four adult MyHC isoforms have been identified in mouse, rat, guinea pig and rabbit skeletal muscles: types I, IIa, IIx and IIb [11, 12]. These four isoforms allow the characterization not only of the four main pure muscle fibre types I, IIA, IIX and IIB, but also hybrid fibre types containing several myosin isoforms, such as type I-IIA, type IIA-IIX or type IIX-IIB fibres. These hybrid fibres signal the change from one pure type into another, driven by a change in age, physical activity levels, or exposure to prolonged stress [2, 6].

Muscles generally comprise various proportions of each muscle fibre type, depending on the muscle function. Insight in the muscle fibre composition is of great importance in a wide range of scientific fields, such as clinical research, biomechanics, and muscle food science. Histoenzymology methods are most often used to characterize the myofibre type on serial muscle cross sections. [13] [14]. However, the use of monoclonal antibodies (mAbs) against myosin heavy chain (MyHC) isoforms enabled a more precise classification of fibres I, IIA, IIX and IIB [12, 15]. One major utility of using mAbs is the delineation of hybrid fibres (I–IIA, IIA–IIX and IIX–IIB), which simultaneously express different isoforms of MyHC inside the same fibre [2].

This intracellular composition that varies depending on the fibre type is likely to change the optical properties of endogenous fluorophores naturally contained in biological cells. It is indeed known that the molecular environment of fluorophores changes their spectral responses [16]. This property has been exploited to

characterize skeletal muscle by the front face fluorescence [17].

However, the low spatial resolution of this technique allows an analysis only of the whole tissue. Moreover, sample excitation in the deep ultraviolet range (200–350 nm) is not straightforward, and it is difficult to highlight some interesting fluorophores. Nonetheless, several fluorescent microscopy techniques can be used. Super-resolution fluorescence microscopy [18-20] use labeled structure of resolution higher than the diffraction limited resolution (Abbe law). The main Super-resolution fluorescence microscopies are based on fluorescent markers, e.g. STED (Stimulated Emission Depletion), PALM (Photo-Activated Localization Microscopy) or STORM (Stochastic Optical Reconstruction Microscopy). Multiphoton microscopy offers another alternative approach for live tissue visualisation of autofluorescent compounds[21-23]. The two infrared photons exciting the sample allow deep tissue penetration in the optical window of living tissue. Finally, the coupling of a deep UV (DUV) fluorescence spectrofluorimeter to a microscope is a another approach allowing a fine characterization of biological tissues at the microscopic scale [24, 25]. Like front-face fluorescence, DUV microspectroscopy needs no external specific probes or labelling, but instead allows the use of the intrinsic fluorescence that many biomolecules display when excited at wavelengths below 350 nm. Compared to DUV monophotonic excitation, high intensities (STED) or long irradiation times (PALM/STORM) are routinely required for Super-resolution fluorescence microscopy. Thus, photo-damaged (bleaching, phototoxicity) are often observed. Moreover, no marker is required in DUV and the maximum resolution reach is around 125 nm (due to DUV excitation range). Multiphoton microscopy also presents some disadvantages (i) being a non-linear process relying onto infrared photons, its resolution remains in the µm range, (ii) the two photon action spectra are very broad and do not permit a fine selectivity, (iii) a large flux of infrared photons is necessary to make two-photon excitation happen, which strong infrared absorption by the tissue can cause irreversible beam damage.

In particular, changes in cellular metabolism can be assessed by observation of flavin adenine dinucleotide, nicotinamide adenine dinucleotide (NADH), tyrosine, tryptophan, or porphyrins [24, 25]. The DISCO beamline of the SOLEIL synchrotron has developed a DUV fluorescence microscope coupled to a synchrotron beamline, providing fine-tuneable excitation from 180 to 600 nm and full-spectrum acquisition from each point scanned, to study DUV-excited fluorescence emitted from nanovolumes directly inside live cells or tissue biopsies [24, 25]. This DUV set-up delivers low energy (tens of microwatts) to the sample and prevents any beam damage.

Given the differences in composition of the different muscle fibre types, our goal was to explore the respective autofluorescence response of muscle fibres previously identified from their metabolic and contractile types.

## Materials and methods

### Biological material

Rats were purchased from Janvier (St-Berthevin, France) and housed at our animal facility (Installation Expérimentale de Nutrition, Unité de Nutrition Humaine, INRA Theix, agreement No. C 63345.14) until sacrifice. To respect animal welfare, the rats were euthanized under anesthesia, without pain nor suffering, in strict accordance with the recommendation of the Regional Ethics Committee (C2E2A N°2) which takes into account the rule of the 3Rs (Replacement, Reduction, Refinement). Four male *Wistar* rats aged 5 months (400–450 g) were anesthetized by isoflurane gas and decapitated with a guillotine. The skin of the lower limbs was immediately removed and the hind limbs were dissected. Extensor digitorum longus (EDL) and soleus muscles were taken from tendon to tendon, taking care to avoid damage. Three of these rats were used for ultrastructural analyses, and the fourth for the DUV microspectroscopy measurements.

### Light microscopy (histology and microspectroscopy)

*Sample preparation*

The muscle part remaining from TEM sampling was positioned on a cork plate with embedding medium (Tissue-Tek), and frozen in isopentane cooled to −160 °C with liquid nitrogen (−196 °C). Serial cross-sections (10 µm thick) cut using a cryostat (Microm, HM 560) were collected on glass slides for histological stains, and on quartz coverslips (ref. CNO.WIN-30-0.17-UV, Laser Components, 92190 Meudon, France) for DUV microspectroscopy fluorescence acquisitions. We deliberately reduced the number of sections to limit erosion of the muscle block, so as to identify the compounds and fibres from the first to the last studied section, enabling reliable composition and morphology identifications. Sections for DUV microspectroscopy were not stained, and were stored at −20 °C under vacuum until analyzed on the synchrotron beamline.

*Visualization of muscle fibres and intramuscular connective tissue*

Sections were stained with Picrosirius red, which shows the intramuscular connective tissue in red, and muscle fibres in yellow [26].

*Metabolic type of muscle fibres*

The oxidative metabolism of individual muscle fibres was shown by a histoenzymology technique revealing the activity of mitochondrial succinyl dehydrogenase (SDH), [27] an enzyme of the Krebs cycle, and therefore characteristic of oxidative metabolism. The SDH catalyzes the conversion of succinic acid to fumaric acid, and causes the reduction of Nitro blue tetrazolium (NBT), which turns blue. Oxidative muscle fibres are stained dark blue, and glycolytic fibres pale blue. As SDH is located in the mitochondria, it also localizes these organelles in the cells.

*Fibre type determination*

The different fibre types were identified by immunohistofluorescence using monoclonal antibodies specific to myosin heavy chain isoforms characteristic for the cell type. The fibre typing was done according to Schiaffino et al., 1989, with slight modifications. Briefly, slow and fast myosin heavy chain isoforms (MyHC) were identified using mouse monoclonal antibodies specific to MyHC isoforms BA-D5 (MyHC-I)

(AGRO-BIO France), SC-71 (MyHC-IIA) (AGRO-BIO France) and BFF3 (MyHC-IIB)(AGRO-BIO France). Myofibre subtypes I, IIA, IIB and hybrid IIX-IIB were deduced according to their response to the different antibodies, and the unmarked cells corresponded to types MyHC-IIX. The different primary MyHC antibodies were visualized by an Alexa Fluor 488 labeled goat anti-mouse IgG secondary antibody (A 11001, Invitrogen). The cell outlines were stained using a rabbit anti-laminin primary polyclonal antibody (L9393 Sigma), and a goat anti-rabbit IgG Cy3-labeled secondary antibody (111-165-008, Jackson).

To show the antigenic expression in muscle tissue, the cross-sections were incubated with both primary antibodies against MyHC and laminin in a humidified box overnight at 4 °C. After washing, primary antibody binding was visualized by incubating for 1 hour in the dark at room temperature with both labeled secondary antibodies (Alexa 488 anti-mouse IgG and CY3 anti-rabbit IgG). Controls were run without the first antibody to validate the results.

*Observations and image acquisition*

Observations and image acquisitions were performed using a photonic microscope (Olympus BX 61) coupled to a high resolution digital camera (Olympus DP 71) and the Cell F software. Picrosirius red stained section images were acquired in bright field mode, and immunohistofluorescence images in fluorescence mode (Cyanine 3: 550/570 nm; Alexa Fluor 488: 495/519 nm).

*Fibre type proportion*

The proportion of each fibre type was determined on the whole muscle cross section. The percentage of each muscle fibre type was calculated according to Meunier et al. (2010) using the Visilog 6.7 Professional image analysis software (Noesis, Gif-sur-Yvette, France).

*Spotting and identification of cell types*

Myofibre types, identified by immunohistochemistry, were localized on the unstained serial sections prepared for DUV microspectroscopy measurements. Each myofibre, characterized by its cell type, was identified with a number. From 7 to 10 cells of each type were analyzed by DUV microspectroscopy.

### DUV microspectroscopy analysis

*Spectral acquisitions*

Synchrotron DUV microspectroscopy was performed on the DISCO beamline of the SOLEIL synchrotron radiation facility (Saint-Aubin, France) [24, 28]. DUV monochromatized light (typically between 270 and 330 nm) was used to excite tissue sections through a 40x ultrafluar immersion objective (Zeiss, Germany). The emission spectra were acquired from 290 to 540 nm, and recorded with a spectral resolution of 0.1 nm. The fluorescence spectrum arising from each excited pixel was recorded. On each selected cell, 20 acquisitions with spatial resolution 1 µm and acquisition time 20 s per spectrum were made in the intracellular space. Of these 20 acquisitions, 10 were acquired in the central part of the cells and 10 on the cell periphery to target mitochondria from the subsarcolemmal space, and from the superficial myofibrillar region located at the periphery of the intracellular space, near the sarcolemma [29]. These last spectral acquisitions were performed several micrometers from the plasma membrane to avoid overflow from the extracellular space. An excitation wavelength of 275 nm was selected for a broad range excitation of intrinsic fluorochromes [24].

*Spectra treatments and statistical analysis*

Autofluorescence spectra were spike- and noise-filtered using an in-house program written in MATLAB version 7.3 (The MathWorks, Natick, MA). The Unscrambler software (v9.8, Camo Software AS, Norway) was used to perform a baseline adjustment to zero and apply unit vector normalization. Processed spectra were analyzed by principal component analysis (PCA). PCA was applied as an unsupervised approach, in order to handle this new set of data and reveal variances or combinations of variables in this large multivariate data set. For this study, the fluorescence spectral domain was reduced to 290–540 nm. The number of possible components was always left sufficiently high (10). After analysis, the family label of each spectrum was obtained and the two first components were plotted. The mean characteristic spectrum of each group was also plotted to relate the separation to spectral features. Score plots were used to show similarity maps, allowing a comparison of spectra regardless of sample categories. Loading plots derived from the first and second principal component X-loading plots were used to obtain and identify characteristic fluorescence peaks. The fluorescence intensity for a wavelength of interest, revealed by the maximum and the minimum of PC loadings, was expressed as mean ± standard error of the mean (SEM). Variance analysis and mean comparisons were performed using one-way variance analysis and the Tukey test under the XLSTATsoftware 2010 (Microsoft office, Redmond, USA).

## Results and discussion

### Muscle fibre characterization

The goal of this work was to accurately identify the type of each muscle cell. For this we used an immunohistofluorescence technique based on the specific recognition of the different isoforms of myosin heavy chains by monoclonal antibodies [6, 11, 30]. This technique is recognized as being particularly reliable. However, we validated the identification by revealing the in situ succinyl dehydrogenase (SDH) activity which is characteristic of oxidative metabolism (and therefore highlighting type I and IIA fibres). The SDH staining matches perfectly with the immunohistofluorescence identification and reconstructed image mapping (**Figure 1**), highlighting the robustness of the fibre type identification.

As expected, immunolabeling and enzymatic activity of SDH indicate that the soleus muscle had only oxidative metabolism fibres (66% type I and 34% type IIA), while the EDL muscle contained four types of pure fibre and hybrid IIX-IIB (4% of type I fibres, 18% type IIA fibres, 24% type IIX fibres, 48% type IIB fibre and 6% type IIX-IIB fibres) (**Figure 1**).

Whichever the muscle studied, the SDH activity was more pronounced in type IIA than in type I fibres (**Figures 1 & 2**), as is usually observed in rat muscles [31, 32]

The distribution of EDL fibre types is close to results found in the literature of around 4% type I, 18% type IIA and 78% glycolytic fibres (including IIX and IIB fibres) [31, 33]. Literature data on soleus muscle are more heterogeneous, with type I fibres ranging from 54% to 90–97% depending on the biological criteria of the rats used in different studies [33-35]. Our results are in this range and are closer to those of Cornachione et al. (2010), who observed

54% type I fibres, 34% IIA fibres in the soleus muscle of adult female Wistar rats, the remaining fibres being considered as hybrid.

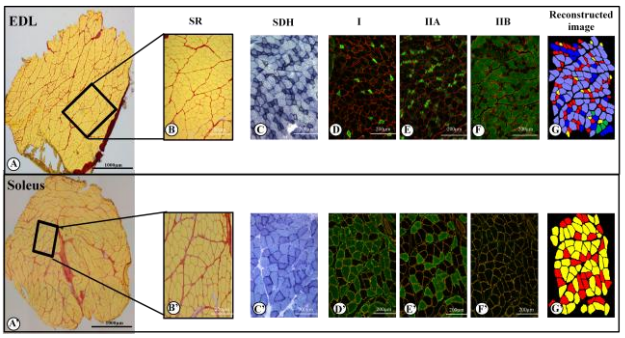


Fig. 1 Histological characterisation of muscles fibre types

Whole muscle cross sections of EDL (A) and soleus (A') muscles stained with Picrosirius red. Muscle fibres are stained in yellow and intramuscular connective tissue in red. For each muscle, all other sections are cut serially, allowing multiple characterization of the same cells. (B & B'): higher magnification of an area of A & A'. (C & C'): SDH staining highlighting the mitochondrial succinyl dehydrogenase activity which is much more pronounced in oxidative fibres (I & IIA fibre types) than in glycolytic ones (IIB & IIX fibre types). (D-F & D'-F'): Each muscle fibre type was identified by immunohistofluorescence using monoclonal antibodies specific for MyHC isoforms (green fluorescence) and an anti-laminin antibody to highlight the cell periphery (orange fluorescence). (G & G'): From all immunohistofluorescence images, a virtual image is reconstructed showing the precise identification of each fibre type.

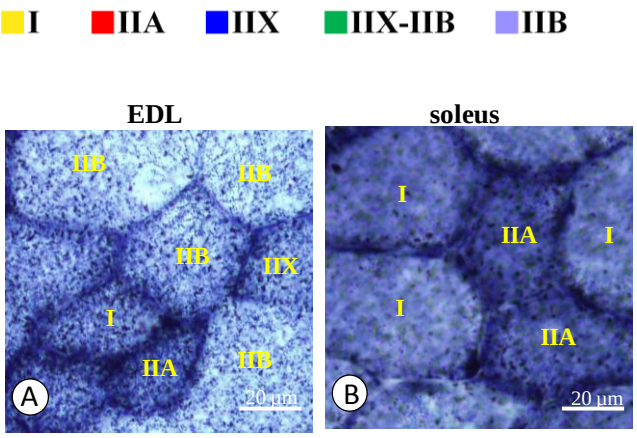


Fig. 2 Mitochondria distribution in EDL and soleus muscles fibres

(A & B): Succinyl dehydrogenase (SDH) staining of transverse muscles sections of EDL and soleus respectively with fibre type initially determined by immunohistofluorescence (light microscopy). Intensity of blue staining reflects the mitochondrial succinyl dehydrogenase activity and consequently the mitochondrial location and density in the muscle cells. Glycolytic fibres are paler than oxidative one showing dark blue coloration. Type IIA fibres express a higher SDH activity than type I fibres. I, IIA, IIB, IIX: type I, IIA, IIB, IIX fibre respectively

## DUV microspectrofluorescence

*DUV fluorescence spectra profile*

Whatever the fibre type and cell localization, all spectra show the same shape (**see Figure S1** as supplementary material). An example of the intracellular spectra acquisition areas (central and periphery), and a typical spectrum, are shown in **Figure 3**.

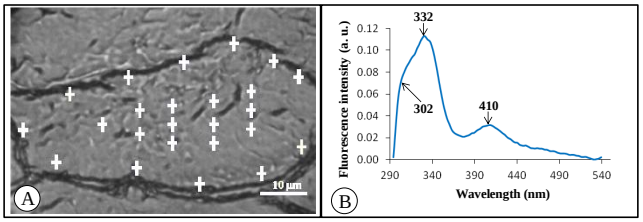


Fig. 3 Intracellular spectra acquisition areas

A: Transverse section of a muscle fibre where each intracellular cross represents a spectrum acquisition. For each cell analyzed, 12 spectra were acquired in the central part of the cell and 12 on the periphery. B: Representative UV fluorescence spectra of rat muscle fibre. The UV spectra show peaks at 332 nm and 410 nm with shoulders at 302 nm. Fluorescence emission at 302 and 332 are assigned to tyrosine and tryptophan respectively. Compound emitting at 410 nm could be NADH.

The spectrum shows two peaks at 332 and 410 nm with a shoulder at 302 nm. The fluorescence emissions at 302 nm and 332 nm are assigned to tyrosine (Tyr) and tryptophan (Trp) respectively [17, 25, 36, 37]. In the literature, fluorescence emission around 410 nm is usually assigned to collagen or elastin [25], but these proteins are specific to the extracellular space, and are completely absent from the intracellular space where the measurements were made. The excellent spatial resolution of the system (1 micron) rules out the possibility that such a strong signal was captured from the extracellular space. This result thus suggests that an intracellular compound has an autofluorescence emission in the same wavelength range as collagen and elastin. It could be related to NADH which is present in muscle cells, especially when oxidative metabolism is dominant [9]. NADH autofluoresces when excited at 260 nm [25], close to the excitation wavelength used in this experiment (275 nm). While free NADH solubilized in PBS has a maximal emission at 460 nm [25], NADH emission fluorescence spectra in the muscle cells can shift to about 410 nm because of the intracellular environment [24, 25].

*Effect of spectra location on autofluorescence response*

Our objective was to investigate the fluorescence response in the periphery compared to internal part of the intracellular space (i.e. subsarcolemmal space). Indeed, the mitochondrial density is usually high in the subsarcolemmal space of muscle fibres, especially in oxidative metabolic I and IIA fibres [29, 38, 39]. Whichever the muscle considered, no significant discrimination was observed between the spectra acquired in the periphery and those acquired in the central part of the cells (**Figure 4**).

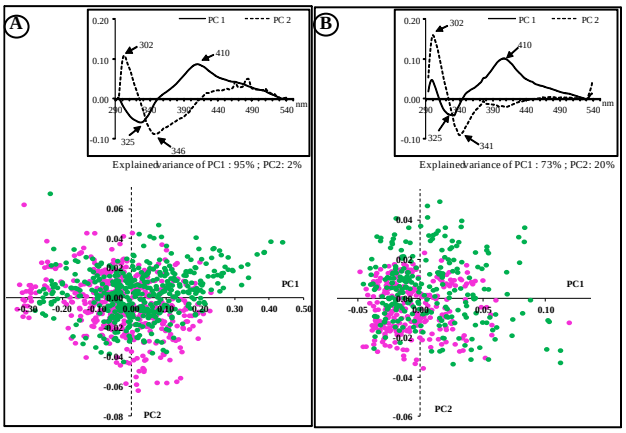


Fig. 4 Effect of the spectra acquisition area on autofluorescence response

PCA score plot of PC1 and PC2 show no discrimination between spectra acquired in the periphery or in the central part of the muscle fibre intracellular spaces. The loadings inform on the wavelengths explaining the largest variability along the X axis (PC1) and along the Y axis (PC2).

● **Central** ● **Periphery**

This result was at first sight surprising as the mitochondrial inner membrane is rich in NADH, responsible for transporting electrons and we expected a higher NADH fluorescence in this region than in the rest of the cell. Later, the results of SDH staining (**Figures 1and 2)**, which highlights mitochondria, and electron microscopy (**See Figure S2** as supplementary material) confirmed a high density of these organelles at the edge of the oxidative muscle fibres. The subsarcolemmal space which has a high density of mitochondria is usually about 2 microns depth [29, 39]. In our experiment, the spectra were acquired a few microns apart from the plasma membrane, to avoid overflow onto the extracellular space. Thus it is possible that edge spectra were acquired outside the subsarcolemmal space. This could explain the absence of discrimination between the spectra acquired in the central part or in the periphery of the cells. Moreover, SDH staining demonstrated a high content of mitochondria in the whole sarcoplasm which attenuates expected differences in mitochondria density between edge and central part of cells.

*Autofluorescence response by fibre type*

Our goal was to investigate and compare the fluorescence emission response of each fibre type when excited at 275 nm. Our results show a clear discrimination between different cell types (**Figures 5 & 6**). Although the groups were well separated, considering the whole data set (data not shown), the separation was even clearer when only the spectra acquired in the central part of cells were taken into account. PCA score plots show a separation on PC2 of slow-twitch fibres (type I) from fast-twitch (type II) (**Figure 5 A, B**) at the loadings highlighting 302 nm and 346 nm as the wavelengths of largest variability. To a lesser extent, oxidative fibres (I, IIA) are separated from glycolytic fibres (IIX, IIB & IIX-IIB) on PC1 at 410 and 325 nm (**Figure 5 A**). Data on metabolic type are available only for the EDL muscle, since soleus muscle contains 100% oxidative fibres.

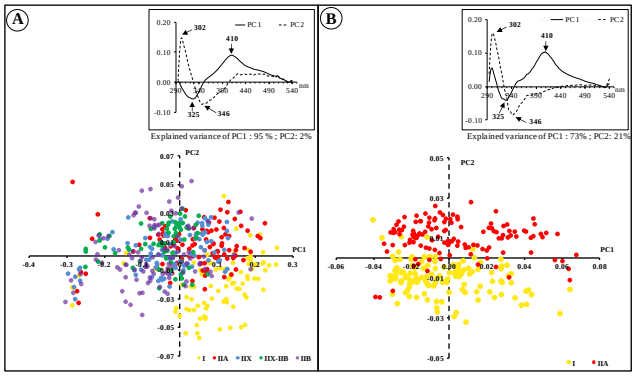


Fig. 5 Autofluorescence response regarding the fibre type (spectra of fibres central part)

PCA score plots and loading of PC1 and PC2 from the four pure types of fibre (I, IIA, IIX, and IIB) and hybrids IIX-IIB in EDL (A) and from the two pure fibre types (I and IIA) in Soleus (B). On both muscles, the contractile type I (slow-twitch) and II (fast-twitch) are well separated along PC2. Compared to type I, type II shows higher fluorescence intensity at 410 nm and a lower intensity at 325 nm. In the score plot of the EDL (A), oxidative fibres (I and IIA) are separated from glycolytic fibres (IIX, IIB & IIX-IIB) along the PC1 axis. Glycolytic fibres show higher fluorescence intensity at 302 nm and a lower intensity at 346 nm. The analysis does not discriminate between glycolytic fibre types.

● **I** ● **IIA** ● **IIX** ● **IIX-IIB** ● **IIB**

Emission fluorescence at 302 nm is assigned to tyrosine, while emission fluorescence at 325 and 346 nm could originate from slight shifts in the emission fluorescence of tryptophan from 332 to 325 and to 346, related to its insertion in specific structural motifs of proteins which affect its physicochemical environment [16, 40]. These changes in Tyr and Trp fluorescence features suggest a strong variation of protein polar environment. The emission fluorescence at 410 nm could be assigned to NADH as discussed above.

On EDL muscle, fluorescence intensity decreased with glycolytic metabolism type and contraction speed at 410 nm, while it increased at 325 nm (**Figure 6**). These differences between fibre types were amplified by analyzing the 410/325 ratio, which decreased in the order I>IIA>IIX>IIX-IIB>IIB. However, the fluorescence intensity of hybrids IIX-IIB, although located between the IIX and IIB, was not significantly different from pure types (IIX and IIB). This difference was not highlighted on the soleus. Of note, the low intrinsic fluctuations most certainly result from analysis performed at selected wavelengths, whereas PCA take into account the whole spectrum. The muscle fibres I and IIA of this muscle had a fluorescence intensity at 410 nm 4 times lower than EDL type I & IIA fibres. Lastly, the fluorescence intensity of type I fibres was higher at 346 nm and lower at 302 nm than type IIA fibres, in both soleus and EDL.

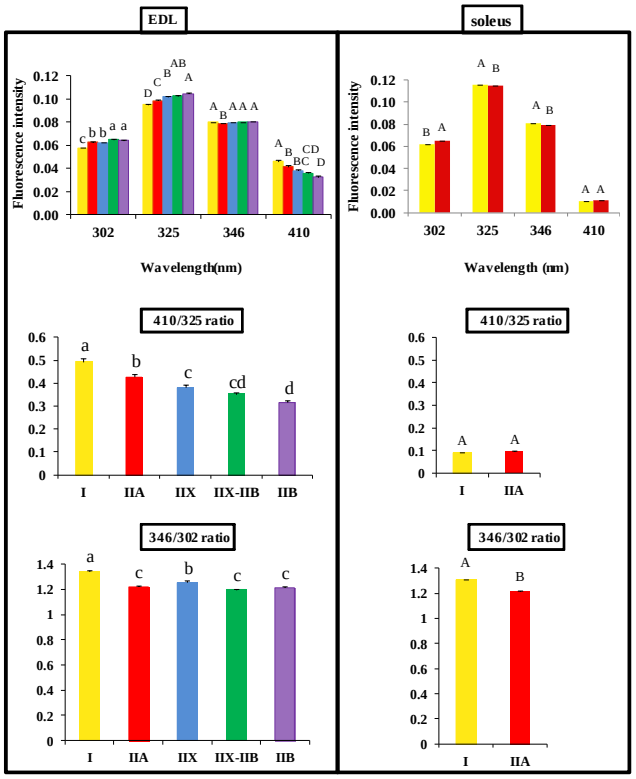


Fig. 6 Fluorescence intensity of fibre types against wavelength evidenced by PCA loadings

On EDL muscle, fluorescence intensity decreases with glycolytic metabolism and contraction speed at 410 nm, and increases at 325 nm. Soleus muscle has only oxidative fibre types with slow-twitch (Type I) and fast-twitch (Type IIA) fibres. On soleus muscle, fluorescence intensity at 410 nm is lower than in EDL muscle, and this wavelength is not discriminating. However, fluorescence intensity is lower at 346 nm and higher at 302 nm for soleus type IIA fibres than for soleus type I fibres. The ratio 410/325 amplifies the differences between EDL muscle fibre types. The ratio 346/302 separates type I fibres from type II fibres in both EDL and soleus. For a given wavelength (top histograms) and wavelength ratio comparisons (bottom histograms), different lowercase letters and capital letters indicate a significant difference for $p < 0.05$ and p<0.01respectively.

I IIA IIX IIX-IIB IIB

Discrimination of contractile types (I versus II) in the central part of cells suggests differences in myofibrillar proteins composition. Some proteins vary in their isoform content depending on their contractile type, the best known being myosin. A comparison of the myosin isoform amino acid sequences of muscle fibres shows more Tyr in type I than in type II fibres, at variance with the higher autofluorescence emission at 302 nm observed in type II than in type I fibres. Although myosin is the most abundant protein in myofibrillar material, other proteins are present with different isoforms depending on the fibre type. The myosin binding proteins such as C-protein, M-protein or titin [30, 41-43], or the thin filament proteins such as tropomyosin or troponins [6, 44, 45] exist in different isoforms depending on the contractile type of the fibre. The differences in tyrosine and tryptophan content and their position in protein molecules, could explain a large part of the autofluorescence variation between Type I and Type II fibres.

As the metabolism became more and more glycolytic in the different types, the fluorescence intensity at 410 nm decreased and that at 325 nm increased (**Figure 6**). The decrease in fluorescence intensity at 410 nm with glycolytic metabolism strengthens our hypothesis that emission of fluorescence at 410 nm comes from NADH. Indeed, NADH is largely contained in the mitochondria [8, 9], whose role is to generate energy by the oxidative pathway. The more the preferential pathway moves towards a glycolytic metabolism, the more the number of mitochondria decreases (which is well illustrated by the SDH staining of Figures 1 and 2) and therefore the amount of NADH decreases, which is consistent with the observed decrease fluorescence intensity at 410 nm in glycolytic fibres compared to oxidative fibres.

Moreover, the preferential metabolic pathway, oxidative or glycolytic, is associated with the numerous enzymes and carriers of these respective pathways. The spectral differences observed at 325 nm (assigned to Trp) could be due to the fact that compared with oxidative fibres, glycolytic fibres just contain more Trp in their proteins.

However, the autofluorescence of endogenous fluorophores is affected more by their molecular and physicochemical environment than by their concentration. The autofluorescence of a compound does not depend only on its concentration, the physicochemical environment having a considerable influence on peak positions and intensity [16, 40]. Therefore, a large part of the variation observed in autofluorescence emission of different fibre types probably results from differences in their overall composition and molecular environment.

## Conclusion

DUV fluorescence microspectroscopy has demonstrated its effectiveness for characterizing muscle tissue. For the first time, muscle cells of different type have been discriminated on a tissue section by exploiting the variation in their autofluorescent spectral responses without adding exogenous markers.

Following excitation at 275 nm, pure muscle fibre types shown varying spectral responses at 302 nm band assigned to tyrosine, fluorescence peaks at 325 and 346 nm, assigned to tryptophan with different molecular environments, and 410 nm which could be a shifted NADH fluorescence emission. The structure and composition of a muscle cell are adapted to its function. Depending on the cell tasks, and therefore on the fibre type, the intracellular compartment presents differences in metabolic pathways, contractile proteins, and overall cytoskeleton appropriate to meeting the cell needs. Therefore, the content of specific protein isoforms, soluble sarcoplasmic molecules, or even components of cellular organelles and sarcoplasmic reticulum may modulate the autofluorescence response of cells. While it appears the discriminatory wavelengths depend on the muscle type, the vast majority of muscles contained a mix of oxidative and glycolytic fibers such as the EDL. As a future research direction, a full overview of the method for cellular profiling could be performed in a broad range of muscle types. Until now, no evidence has shown whether these changes in

fluorescence intensity as a function of contractile and metabolic types are related to differences in the concentration of fluorophores identified, including Trp and Tyr, or to their environment. These results suggest that the UV autofluorescence features of muscle cells could be used in the future for their characterization. Moreover, they complement the NADH studies for cell differentiation by FLIM [46], suggesting that label-free fluorescence imaging is indeed a very powerful alternative to vibrational spectroscopic methods and pave the way for cellular in vivo differentiation. DUV microspectrosopy and FLIM are really complementary. Fluorescence lifetime being very sensitive to fluorochromes surrounding [47], becomes a reliable marker of metabolic events and its variations are independent of the number of emitters [16, 40]. On the other hand, DUV microspectroscopy can follow numerous different autofluorescent markers at the same time (aromatic aminoacids, NADH, collagen crosslinks, elastin, …) and provides a corpus of fingerprints that may be linked for differentiation to changes in cellular micro-environment and concentration in fluorochromes with lesser contrast sensitivity than FLIM but stronger versatility. Future developments using laser and laboratory microscopes [48] may allow the implementation of DUV fluorescence microspectroscopy routine analysis free of synchrotron radiation.

## Notes and references

[a] *INRA, UR370 Qualité des Produits Animaux, F-63122 Saint-Genès-Champanelle, France.*
[b] *INRA, UR454 Microbiologie, F-63122 Saint-Genès-Champanelle, France*
[c] *Synchrotron SOLEIL, BP48, L'Orme des Merisiers, F-91120 Gif-sur-Yvette, France*
[d] *INRA, UAR1008 CEPIA, rue de la Géraudière, F-44316 Nantes, France*
*Thierry.astruc@clermont.inra.fr*

Acknowledgments

This work was supported by INRA (French National Institute for Agronomical Research) with the MICEL project funded by the inter-division CEPIA/MICA (Science and Process Engineering of Agricultural Products/Microbiology and Food Chain). Experiments were performed at the SOLEIL synchrotron on the DISCO beamline in the framework of project No. 20120364. The authors thank Dr Alain Buleon for support and helpful discussions, and Christophe Delhomme and the team of "Installation Experimentale de Nutrition" (INRA Theix, 63122 St-Genès-Champanelle) for housing rats and for technical assistance during sacrifice. Dr Caroline Chagnot was a PhD Research Fellow funded by the "Région Auvergne CPER (Contrat de Projet État-Région) – FEDER (Fonds Européen de Développement Régional)".

† Electronic Supplementary Information (ESI) available: [Electron microscopy of rat EDL muscle]. See DOI: 10.1039/b000000x/

1. T. Astruc, in *Encyclopedia of Meat Science*, eds. C. Devine and M. Dikeman, Elsevier, Oxford, 2 edn., 2014, vol. 2, pp. 442-448.
2. D. Pette and R. S. Staron, *Reviews of physiology, biochemistry and pharmacology*, 1990, 116, 1-76.
3. L. Lefaucheur, *Meat Sci*, 2010, 84, 257-270.
4. Y. M. Choi and B. C. Kim, *Livestock Science*, 2009, 122, 105-118.
5. S. Schiaffino and C. Reggiani, *Physiol Rev*, 1996, 76, 371-423.
6. S. Schiaffino and C. Reggiani, *Physiol Rev*, 2011, 91, 1447-1531.
7. F. Chemello, C. Bean, P. Cancellara, P. Laveder, C. Reggiani and G. Lanfranchi, *PLoS One*, 2011, 6, e16807.
8. A. Mayevsky and G. G. Rogatsky, *Am J Physiol-Cell Ph*, 2007, 292, C615-C640.
9. J. M. Ren, J. Henriksson, A. Katz and K. Sahlin, *Biochem J*, 1988, 251, 183-187.
10. Y. Ogura, H. Naito, R. Kakigi, N. Ichinoseki-Sekine, M. Kurosaka and S. Katamoto, *Biochemical and Biophysical Research Communications*, 2008, 372, 584-588.
11. A. Bar and D. Pette, *FEBS Lett*, 1988, 235, 153-155.
12. S. Schiaffino, L. Gorza, S. Sartore, L. Saggin, S. Ausoni, M. Vianello, K. Gundersen and T. Lomo, *J Muscle Res Cell Motil*, 1989, 10, 197-205.
13. M. H. Brooke and K. K. Kaiser, *J Histochem Cytochem*, 1970, 18, 670-672.
14. C. R. Ashmore and L. Doerr, *Exp Neurol*, 1971, 31, 408-418.
15. B. Picard, M. P. Duris and C. Jurie, *Histochem J*, 1998, 30, 473-479.
16. J. R. Lakowicz, *Principles of Fluorescence Spectroscopy*, Springer (Eds), Boston (USA), 3rd edn., 2006.
17. A. Sahar, T. Boubellouta, J. Lepetit and E. Dufour, *Meat science*, 2009, 83, 672-677.
18. P. J. Walla, ed. W. P. J., Wiley-JCH verlag GmbH, Weinheim, Germany, second edition edn., 2014.
19. S. W. Hell, *Nat Methods*, 2009, 6, 24-32.
20. L. Schermelleh, R. Heintzmann and H. Leonhardt, *J Cell Biol*, 2010, 190, 165-175.
21. W. R. Zipfel, R. M. Williams, R. Christie, A. Y. Nikitin, B. T. Hyman and W. W. Webb, *P Natl Acad Sci USA*, 2003, 100, 7075-7080.
22. W. Denk, J. H. Strickler and W. W. Webb, *Science*, 1990, 248, 73-76.
23. D. W. Piston, *Trends Cell Biol*, 1999, 9, 66-69.
24. F. Jamme, S. Villette, A. Giuliani, V. Rouam, F. Wien, B. Lagarde and M. Refregiers, *Microsc Microanal*, 2010, 16, 507-514.
25. F. Jamme, S. Kascakova, S. Villette, F. Allouche, S. Pallu, V. Rouam and M. Refregiers, *Biol Cell*, 2013, 105, 277-288.
26. A. Liu, T. Nishimura and K. Takahashi, *Meat science*, 1995, 39, 135-142.
27. M. M. Nachlas, K. C. Tsou, E. De Souza, C. S. Cheng and A. M. Seligman, *J Histochem Cytochem*, 1957, 5, 420-436.
28. A. Giuliani, F. Jamme, V. Rouam, F. Wien, J. L. Giorgetta, B. Lagarde, O. Chubar, S. Bac, I. Yao, S. Rey, C. Herbeaux, J. L. Marlats, D. Zerbib, F. Polack and M. Refregiers, *J Synchrotron Radiat*, 2009, 16, 835-841.
29. J. Nielsen, M. Mogensen, B. F. Vind, K. Sahlin, K. Hojlund, H. D. Schroder and N. Ortenblad, *Am J Physiol Endocrinol Metab*, 2010, 298, E706-713.
30. M. Gautel, D. O. Furst, A. Cocco and S. Schiaffino, *Circ Res*, 1998, 82, 124-129.
31. D. Bloemberg and J. Quadrilatero, *PloS one*, 2012, 7.
32. K. Punkt, A. Naupert and G. Asmussen, *Acta Histochem*, 2004, 106, 145-154.
33. P. Novak, G. Zacharova and T. Soukup, *Physiol Res*, 2010, 59, 783-801.

34. A. Cornachione, L. O. Cacao-Benedini, E. Z. Martinez, L. Neder and A. Claudia Mattiello-Sverzut, *Acta Histochem*, 2011, 113, 277-282.
35. K. Punkt, H. Mehlhorn and H. Hilbig, *Acta Histochem*, 1998, 100, 37-58.
36. S. Pallu, G. Y. Rochefort, C. Jaffre, M. Refregiers, D. B. Maurel, D. Benaitreau, E. Lespessailles, F. Jamme, C. Chappard and C. L. Benhamou, *PloS one*, 2012, 7, 1-11.
37. L. Theron, A. Venien, F. Jamme, X. Fernandez, F. Peyrin, C. Molette, P. Dumas, M. Refregiers and T. Astruc, *J Agr Food Chem*, 2014, 62, 5954-5962.
38. R. S. Filgueras, T. Astruc, R. Labas, A. Venien, F. Peyrin, R. C. Zambiazi and V. Sante-Lhoutellier, *Food chemistry*, 2012, 132, 1387-1394.
39. T. Yamada, Y. Furuichi, H. Takakura, T. Hashimoto, Y. Hanai, T. Jue and K. Masuda, *J Appl Physiol (1985)*, 2013, 114, 490-497.
40. B. Valeur, *Molecular Fluorescence: Principles and Applications*, Wiley-VCH Verlag GmbH (Eds), 2001.
41. W. M. J. Obermann, M. Gautel, F. Steiner, P. F. M. vanderVen, K. Weber and D. O. Furst, *J Cell Biol*, 1996, 134, 1441-1453.
42. K. Wang, R. Mccarter, J. Wright, J. Beverly and R. Ramirezmitchell, *P Natl Acad Sci USA*, 1991, 88, 7101-7105.
43. R. Horowits, *Biophys J*, 1992, 61, 392-398.
44. R. Bottinelli, D. A. Coviello, C. S. Redwood, M. A. Pellegrino, B. J. Maron, P. Spirito, H. Watkins and C. Reggiani, *Circ Res*, 1998, 82, 106-115.
45. D. Danieli-Betto, R. Betto and M. Midrio, *Pflugers Archiv : European journal of physiology*, 1990, 417, 303-308.
46. C. Stringari, J. L. Nourse, L. A. Flanagan and E. Gratton, *PloS one*, 2012, 7.
47. N. P. Galletly, J. McGinty, C. Dunsby, F. Teixeira, J. Requejo-Isidro, I. Munro, D. S. Elson, M. A. A. Neil, A. C. Chu, P. M. W. French and G. W. Stamp, *Brit J Dermatol*, 2008, 159, 152-161.
48. B. J. Zeskind, C. D. Jordan, W. Timp, L. Trapani, G. Waller, V. Horodincu, D. J. Ehrlich and P. Matsudaira, *Nat Methods*, 2007, 4, 567-569.